Contemporary Mathematics
https://ojs.wiserpub.com/index.php/CM/

Research Article

Stability Analysis, Modulations Instability, Asymptotic Behavior, and Exact Solitons to the *F*-Kpp Equation

Muhammad Raheel[1], Dean Chou[2,3], Asim Zafar[1]*

[1] Department of Mathematics, COMSATS University Islamabad, Vehari Campus, Vehari, Pakistan
[2] Department of Biomedical Engineering, National Cheng Kung University, Tainan, 701401, Taiwan
[3] Academy of Innovative Semiconductor and Sustainable Manufacturing, National Cheng Kung University, Tainan, 701401, Taiwan
E-mail: asimzafar@cuivehari.edu.pk

Received: 1 July 2025; **Revised:** 25 July 2025; **Accepted:** 30 July 2025

Abstract: This paper reveals a nonlinear mathematical Fisher-Kolmogorov-Petrovskii-Piskunov (F-KPP) equation in a biological system. This model has much importance in population genetics as well as nematic liquid crystals, explaining the reaction-diffusion system through traveling waves in population genetics as well as pattern formation in bi-stable systems. We use a fractional derivative to improve accuracy as well as understand the dynamics of the model. By utilizing the modified simplest equation method, we investigate the distinct kinds of exact wave solutions involving trigonometric, hyperbolic, and rational functions. To obtain and verify the solutions, we use the Mathematica software. We demonstrate the obtained solutions through 2-D, 3-D, and contour plots with the use of the Mathematica tool. The main contribution of this paper is to analyze the qualitative analyses, including stability analysis, modulation instability, and asymptotic analysis. At the end, the gained solutions are fruitful in different areas, like ecology, gene mutation, combustion theory, phase transition, and many others.

***Keywords*:** mathematical equation, stability analysis, modulations instability, asymptotic behavior, analytical method, exact solitons

MSC: 35C07, 35C08, 83C15

1. Introduction

The study of nonlinear partial differential equations assists in modeling and understanding physically complicated problems such as wave motion, fluid dynamics, plasma physics, and light propagation in certain media. These equations become useful because they quantify and explain the movement, interaction, and dynamic change of waves in time and space. Fractional derivatives are a mathematical concept that extends the traditional derivative to non-integer orders. They are used to model complex systems and phenomena that exhibit memory or hereditary properties. To improve the accuracy and understanding of the model, different kinds of fractional derivatives are utilized, such as the Caputo fractional derivative [1], the β-time fractional derivative [2], the Riemann-Liouville fractional derivative [3], the Conformable fractional derivative [4], the Caputo-Hadamard fractional derivative [5], and many others.

The concerned space-time F-KPP model is given in [6]:

DOI: https://doi.org/10.37256/cm.6520257660

$$g_t + \nu(g_{xx} + 2g_{xy} + g_{yy}) - (g_x + g_y) + \Im(g) = 0. \tag{1}$$

Here g is a wave function that denotes the chemical concentration depends upon the spatio variables x and y and the temporal variable t. While ν represents a positive diffusion coefficient. Eq. (1) is a type of reaction-diffusion system that may be utilized in population growth and wave propagation models. This model is used in population genetics as well as nematic liquid crystals, explaining the reaction-diffusion system through traveling waves in population genetics as well as pattern formation in bi-stable systems. Eq. (1) is named the Fisher-Kolmogorov-Petrovskii-Piskunov model by Ronald Fisher, Andrey Kolmogorov, Ivan Petrovsky, and Nikolai Piskunov. This model has been discussed by different researchers and mathematicians with the help of different methods, including the modified direct algebraic technique [6], the wavelet collocation scheme [7], the generalized extended direct algebraic technique [8], the $(1/G)$-expansion scheme [9], the regular perturbation technique [10], the modified extended direct algebraic scheme [11], the generalized Sinh-Gordon equation technique [12], etc.

Our concerned scheme is the Modified Simplest Equation (MSE) scheme. This scheme is a mathematical approach applied to obtain exact solitons for nonlinear partial differential equations as well as nonlinear partial fractional differential equations. This method was developed by Nikolay K. Vitanov and others; this methodology has undergone significant developments and extensions. Many models are solved by utilizing this method, including the Whitham-Broer-Kaup equation [13], the Schrödinger-Hirota equation [14], the coupled Boussinesq equations [15], the Konopelchenko-Dubrovsky equation [16], the new Hamiltonian amplitude equation [17], the Radha-Lakshmanan equation [18], etc.

The motivation of our research is to explore the new exact wave solitons of a (2 + 1)-dimensional truncated M-fractional F-KPP model by utilizing the modified simplest equation technique. The concerned model in the concept of truncated M-fractional derivative is helpful to understand the phenomenon. This definition of fractional derivative satisfies the properties of both fractional and integer orders, while the other definitions of fractional derivatives (e.g Caputo or Riemann-Liouville) do not. The truncated M-fractional derivative provides solutions close to the numerical solutions of the concerned model. In the future, the obtained results can be compared with the numerical results of the concerned model given in [19]. Moreover, different analyses, including the stability analysis, modulation instability, and asymptotic analysis of the concerned model, are performed.

There are distinct sections in this paper; technique is explained in Section 2, mathematical analysis and exact wave results are mentioned in Section 3, graphical interpretation is given in Section 4, stability analysis is explained in Section 5, modulation instability is performed in Section 6, asymptotic analysis is described in Section 7, and we conclude in Section 8.

1.1 *Truncated M-fractional derivative*

Definition 1 Suppose $g(y) : [0, \infty) \to \mathbb{R}$, so Truncated M-Fractional Derivative (TMFD) of g of order ε is given in [20]:

$$D^{\varepsilon,\rho}_{M,y} g(y) = \lim_{\varepsilon \to 0} \frac{g\ (y\, E_\rho(\varepsilon y^{1-\varepsilon})) - g(y)}{\varepsilon}, \quad \varepsilon \in (0,\ 1],\ \ \rho > 0, \tag{2}$$

here, $E_\rho(.)$ shows a Truncated Mittag-Leffler (TML) profile [21].

$$E_\rho(z) = \sum_{j=0}^{i} \frac{z^j}{\Gamma(\rho j + 1)},\ \ \rho > 0 \ \text{ and } \ z \in \mathbf{C}. \tag{3}$$

Theorem 1 Suppose $a,\ b$ are the real numbers and $g,\ f$ are ε-differentiable for $y > 0$, from [20]:

$$\text{(a) } D^{\varepsilon,\ \rho}_{M,\ y}(ag(y) + bf(y)) = aD^{\varepsilon,\ \rho}_{M,\ y}g(y) + bD^{\varepsilon,\ \rho}_{M,\ y}f(y). \tag{4}$$

$$\text{(b) } D^{\varepsilon,\ \rho}_{M,\ y}(g(y).f(y)) = g(y)D^{\varepsilon,\ \rho}_{M,\ y}f(y) + f(y)D^{\varepsilon,\ \rho}_{M,\ y}g(y). \tag{5}$$

$$\text{(c) } D^{\varepsilon,\ \rho}_{M,\ y}\left(\frac{g(y)}{f(y)}\right) = \frac{f(y)D^{\varepsilon,\ \rho}_{M,\ y}g(y) - g(y)D^{\varepsilon,\ \rho}_{M,\ y}f(y)}{(f(y))^2}. \tag{6}$$

$$\text{(d) } D^{\varepsilon,\ \rho}_{M,\ y}(C) = 0, \text{ where } C \text{ is a constant.} \tag{7}$$

$$\text{(e) } D^{\varepsilon,\ \rho}_{M,\ y}g(y) = \frac{y^{1-\varepsilon}}{\Gamma(\rho+1)}\frac{dg(y)}{dy}. \tag{8}$$

Like Riemann-Liouville derivative, the truncated M-fractional derivative has a more straightforward definition and is easier to apply in certain contexts. Like Caputo derivative, the truncated M-fractional derivative has a different kernel function, which can be beneficial in certain applications. The truncated M-fractional derivative provides more flexibility in modeling systems with different types of behavior. This definition of fractional derivative is used for many models, including the generalized Kudryashov's equation [22], the Kuralay-II equation [23], the Davey-Stewartson-Kadomtsev-Petviashvili equation [24], etc.

2. Modified simplest equation technique

Some of the steps are given as.

Step 1: Consider a NLPD equation:

$$S(h,\ h^2h_\gamma,\ h_\theta,\ h_{\gamma\gamma},\ h_{\theta\theta},\ h_{\gamma\theta},\ ...) = 0. \tag{9}$$

Supposing a traveling wave transformation:

$$h(\gamma,\ \theta) = H(\upsilon),\ \ \upsilon = \gamma - \lambda\theta. \tag{10}$$

Putting Eq. (10) into Eq. (9), yields;

$$Z(H,\ H^2H^{'},\ H^{''},\ ...) = 0. \tag{11}$$

Step 2: Assuming the result of Eq. (11) mentioned is:

$$H(\mho) = b_0 + \sum_{j=1}^{m} b_j \Psi^j(\mho). \tag{12}$$

Where $b_j (j = 1,\ 2,\ 3,\ ...)$ are to be found where $b_m \neq 0$.
A novel function $\Psi(\mho)$ fulfills this:

$$\Psi'(\mho) = \Psi^2(\mho) + \Delta, \tag{13}$$

where Δ is a constant.

Consider the solutions of Eq. (13) based on Δ:
Case 1: when $\Delta < 0$;

$$\Psi(\mho) = -\sqrt{-\Delta}\tanh(\sqrt{-\Delta}\,\mho). \tag{14}$$

$$\Psi(\mho) = -\sqrt{-\Delta}\coth(\sqrt{-\Delta}\,\mho). \tag{15}$$

$$\Psi(\mho) = \sqrt{-\Delta}(\,-\tanh(2\sqrt{-\Delta}\,\mho) \pm i\,\mathbf{sech}(2\sqrt{-\Delta}\,\mho)). \tag{16}$$

$$\Psi(\mho) = \sqrt{-\Delta}(\,-\coth(2\sqrt{-\Delta}\,\mho) \pm \mathbf{csch}(2\sqrt{-\Delta}\,\mho)). \tag{17}$$

$$\Psi(\mho) = -\frac{\sqrt{-\Delta}}{2}\left(\tanh\left(\frac{\sqrt{-\Delta}}{2}\,\mho\right) + \coth\left(\frac{\sqrt{-\Delta}}{2}\,\mho\right)\right). \tag{18}$$

Case 2: when $\Delta > 0$,

$$\Psi(\mho) = \sqrt{\Delta}\tan(\sqrt{\Delta}\,\mho). \tag{19}$$

$$\Psi(\mho) = -\sqrt{\Delta}\cot(\sqrt{\Delta}\,\mho). \tag{20}$$

$$\Psi(\mho) = \sqrt{\Delta}(\tan(2\sqrt{\Delta}\,\mho) \pm \sec(2\sqrt{\Delta}\,\mho)). \tag{21}$$

$$\Psi(\mho) = \sqrt{\Delta}(\,-\cot(2\sqrt{\Delta}\,\mho) \pm \csc(2\sqrt{\Delta}\,\mho)). \tag{22}$$

$$\Psi(\mho) = \frac{\sqrt{\Delta}}{2}\left(\tan\left(\frac{\sqrt{\Delta}}{2}\,\mho\right) - \cot\left(\frac{\sqrt{\Delta}}{2}\,\mho\right)\right). \tag{23}$$

Case 3: when $\Delta = 0$,

$$\Psi(\mho) = -\frac{1}{\mho}. \tag{24}$$

Step 3: Putting Eqs. (12) and (13) in Eq. (11), and collecting the coefficient of each power of $\Psi(\mho)$. Putting each equal to zero, a system is obtained involving b_j and others. Solve a given set to obtain values.

Step 4: By using Eq. (13) along with the above obtained solutions into Eq. (12), attain the exact solitons for Eq. (9).

There are many merits of the Modified Simplest Equation (MSE) method. Instantly, this method provides a direct and efficient way to find exact solutions of nonlinear PDEs, reducing the complexity of calculations. This method can be used for a broad range of nonlinear PDEs, including those with variable coefficients and nonlinearity. This method can provide insight into the structure of solutions, including the relationship between different terms and the role of nonlinearity. Unlike some numerical methods, this method does not require initial guesses, which can be advantageous in certain situations.

3. Mathematical analysis

In our research, we consider $\Im(g) = g^3 - g$ given in [25] in Eq. (1), we get:

$$g_t + \nu(g_{xx} + 2g_{xy} + g_{yy}) - (g_x + g_y) + g^3 - g = 0. \tag{25}$$

By using the concept of truncated M-fractional derivative, Eq. (25) can be written as:

$$D^{\varepsilon,\,\rho}_{M,\,t}g + \nu(D^{2\varepsilon,\,\rho}_{M,\,x}g + 2D^{\varepsilon,\,\rho}_{M,\,x}(D^{\varepsilon,\,\rho}_{M,\,y}g) + D^{2\varepsilon,\,\rho}_{M,\,y}g) - (D^{\varepsilon,\,\rho}_{M,\,x}g + D^{\varepsilon,\,\rho}_{M,\,y}g) + g^3 - g = 0. \tag{26}$$

$$g(x,\,y,\,t) = G(\mho), \qquad \mho = \frac{\Gamma(\rho+1)}{\varepsilon}(x^\varepsilon + y^\varepsilon + \omega t^\varepsilon). \tag{27}$$

Where, ω represents the wave velocity.

By applying the Eq. (27) into Eq. (26), we get:

$$(\omega - 2)G' + G^3 + 4\nu G'' - G = 0. \tag{28}$$

Applying the homogeneous balance technique and balancing the terms G'' and G^3, we achieve $m = 1$. Now, we will find the exact wave solutions with the use of the modified simplest equation method.

3.1 *Exact wave solutions*

Eq. (12) becomes for $m = 1$:

$$G(\mho) = b_0 + b_1\Psi(\mho). \tag{29}$$

Inserting Eq. (29) in Eq. (28) with Eq. (13) yields.

Set 1:

$$\left\{b_0 = 0,\ b_1 = \pm\frac{1}{\sqrt{-\Delta}},\ \omega = 2,\ \nu = \frac{1}{8\Delta}\right\}. \tag{30}$$

According to the Eqs. (30), (29), (27), and (14), we get:

$$g(x,\ y,\ t) = \mp\frac{1}{\sqrt{-\Delta}}(\sqrt{-\Delta}\tanh(\sqrt{-\Delta}\,\mho)). \tag{31}$$

By applying the Eqs. (30), (29), (27), and (15), then:

$$g(x,\ y,\ t) = \mp\frac{1}{\sqrt{-\Delta}}(\sqrt{-\Delta}\coth(\sqrt{-\Delta}\,\mho)). \tag{32}$$

From the Eqs. (30), (29), (27), and (16), we obtain:

$$g(x,\ y,\ t) = \pm\frac{1}{\sqrt{-\Delta}}(\sqrt{-\Delta}((-\tanh(2\sqrt{-\Delta}\,\mho) \pm i\ \mathbf{sech}(2\sqrt{-\Delta}\,\mho)))). \tag{33}$$

By using Eqs. (30), (29), (27), and (17), then:

$$g(x,\ y,\ t) = \pm\frac{1}{\sqrt{-\Delta}}(\sqrt{-\Delta}((-\coth(2\sqrt{-\Delta}\,\mho) \pm \mathbf{csch}(2\sqrt{-\Delta}\,\mho)))). \tag{34}$$

By utilizing Eqs. (30), (29), (27), and (18), authors gain:

$$g(x,\ y,\ t) = \pm\frac{1}{\sqrt{-\Delta}}\left(-\frac{\sqrt{-\Delta}}{2}\left(\left(\tanh\left(\frac{\sqrt{-\Delta}}{2}\,\mho\right) + \coth\left(\frac{\sqrt{-\Delta}}{2}\,\mho\right)\right)\right)\right). \tag{35}$$

According to the Eqs. (30), (29), (27), and (19), authors obtain:

$$g(x,\ y,\ t) = \pm\frac{1}{\sqrt{-\Delta}}(\sqrt{\Delta}\tan(\sqrt{\Delta}\,\mho)). \tag{36}$$

By using Eqs. (30), (29), (27), and (20), then:

$$g(x,\ y,\ t) = \mp\frac{1}{\sqrt{-\Delta}}(\sqrt{\Delta}\cot(\sqrt{\Delta}\,\mho)). \tag{37}$$

From the Eqs. (30), (29), (27), and (21), we get:

$$g(x,\ y,\ t) = \pm\frac{1}{\sqrt{-\Delta}}(\sqrt{\Delta}(\tan(2\sqrt{\Delta}\,\mho) \pm \sec(2\sqrt{\Delta}\,\mho))). \tag{38}$$

By using Eqs. (30), (29), (27), and (22), then:

$$g(x,\ y,\ t) = \pm\frac{1}{\sqrt{-\Delta}}(\sqrt{\Delta}(\ -\cot(2\sqrt{\Delta}\,\mho) \pm \csc(2\sqrt{\Delta}\,\mho))). \tag{39}$$

By utilizing the Eqs. (30), (29), (27), and (23), then:

$$g(x,\ y,\ t) = \pm\frac{1}{\sqrt{-\Delta}}\left(\frac{\sqrt{\Delta}}{2}\left(\tan\left(\frac{\sqrt{\Delta}}{2}\,\mho\right) - \cot\left(\frac{\sqrt{\Delta}}{2}\,\mho\right)\right)\right). \tag{40}$$

Where $\Theta = \dfrac{\Gamma(\rho+1)}{\varepsilon}(x^{\varepsilon} + y^{\varepsilon} + 2t^{\varepsilon})$.

Set 2:

$$\left\{b_0 = \pm\frac{1}{2},\ b_1 = \pm\frac{1}{2\sqrt{-\Delta}},\ \omega = 2 \mp \frac{3}{4\sqrt{-\Delta}},\ \nu = \frac{1}{32\Delta}\right\}. \tag{41}$$

According to the Eqs. (41), (29), (27), and (14), authors gain:

$$g(x,\ y,\ t) = \pm\frac{1}{2}\left(1 + \frac{1}{\sqrt{-\Delta}}(\sqrt{-\Delta}\tanh(\sqrt{-\Delta}\,\mho)\right). \tag{42}$$

From the Eqs. (41), (29), (27), and (15), we get:

$$g(x,\ y,\ t) = \pm\frac{1}{2}\left(1 + \frac{1}{\sqrt{-\Delta}}(\sqrt{-\Delta}\coth(\sqrt{-\Delta}\,\mho)\right). \tag{43}$$

By using Eqs. (41), (29), (27), and (16), then:

$$g(x,\ y,\ t) = \pm\frac{1}{2}\left(1 - \frac{1}{\sqrt{-\Delta}}(\sqrt{-\Delta}(\ -\tanh(2\sqrt{-\Delta}\,\mho) \pm i\ \mathbf{sech}(2\sqrt{-\Delta}\,\mho))\right). \tag{44}$$

By utilizing the Eqs. (41), (29), (27), and (17), authors obtain:

$$g(x,\ y,\ t) = \pm\frac{1}{2}\left(1 - \frac{1}{\sqrt{-\Delta}}(\sqrt{-\Delta}(\ -\coth(2\sqrt{-\Delta}\,\mho) \pm \mathbf{csch}(2\sqrt{-\Delta}\,\mho))\right). \tag{45}$$

According to the Eqs. (41), (29), (27), and (18), we get:

$$g(x,\ y,\ t) = \pm\frac{1}{2}\left(1 - \frac{1}{\sqrt{-\Delta}}\left(-\frac{\sqrt{-\Delta}}{2}\left(\tanh\left(\frac{\sqrt{-\Delta}}{2}\,\mho\right) + \coth\left(\frac{\sqrt{-\Delta}}{2}\,\mho\right)\right)\right)\right). \tag{46}$$

By using Eqs. (41), (29), (27), and (19), then:

$$g(x,\ y,\ t) = \pm\frac{1}{2}\left(1 - \frac{1}{\sqrt{-\Delta}}(\sqrt{\Delta}\tan(\sqrt{\Delta}\,\mho)\right). \tag{47}$$

From the Eqs. (41), (29), (27), and (20), authors gain:

$$g(x,\ y,\ t) = \pm\frac{1}{2}\left(1 + \frac{1}{\sqrt{-\Delta}}(\sqrt{\Delta}\cot(\sqrt{\Delta}\,\mho)\right). \tag{48}$$

By using Eqs. (41), (29), (27), and (21), then:

$$g(x,\ y,\ t) = \pm\frac{1}{2}\left(1 - \frac{1}{\sqrt{-\Delta}}(\sqrt{\Delta}(\tan(2\sqrt{\Delta}\,\mho) \pm \sec(2\sqrt{\Delta}\,\mho))\right). \tag{49}$$

According to the Eqs. (41), (29), (27), and (22), we obtain:

$$g(x,\ y,\ t) = \pm\frac{1}{2}\left(1 - \frac{1}{\sqrt{-\Delta}}(\sqrt{\Delta}(-\cot(2\sqrt{\Delta}\,\mho) \pm \csc(2\sqrt{\Delta}\,\mho))\right). \tag{50}$$

By utilizing the Eqs. (41), (29), (27), and (23), we achieve:

$$g(x,\ y,\ t) = \pm\frac{1}{2}\left(1 - \frac{1}{\sqrt{-\Delta}}\left(\frac{\sqrt{\Delta}}{2}\left(\tan\left(\frac{\sqrt{\Delta}}{2}\,\mho\right) - \cot\left(\frac{\sqrt{\Delta}}{2}\,\mho\right)\right)\right)\right). \tag{51}$$

Where $\mho = \dfrac{\Gamma(\rho+1)}{\varepsilon}\left(x^{\varepsilon} + y^{\varepsilon} + \left(2 \mp \dfrac{3}{4\sqrt{-\Delta}}\right)t^{\varepsilon}\right)$.

4. Graphical interpretation

In this section, the gained results are demonstrated through two-, three-dimensional, and contour Figures 1-7. The 2-D graphs are shown at $\varepsilon = 0.4,\ 0.8,\ 1$ to represent the effect of TMFD on the gained exact solitons. Moreover, we added the importance of the solutions.

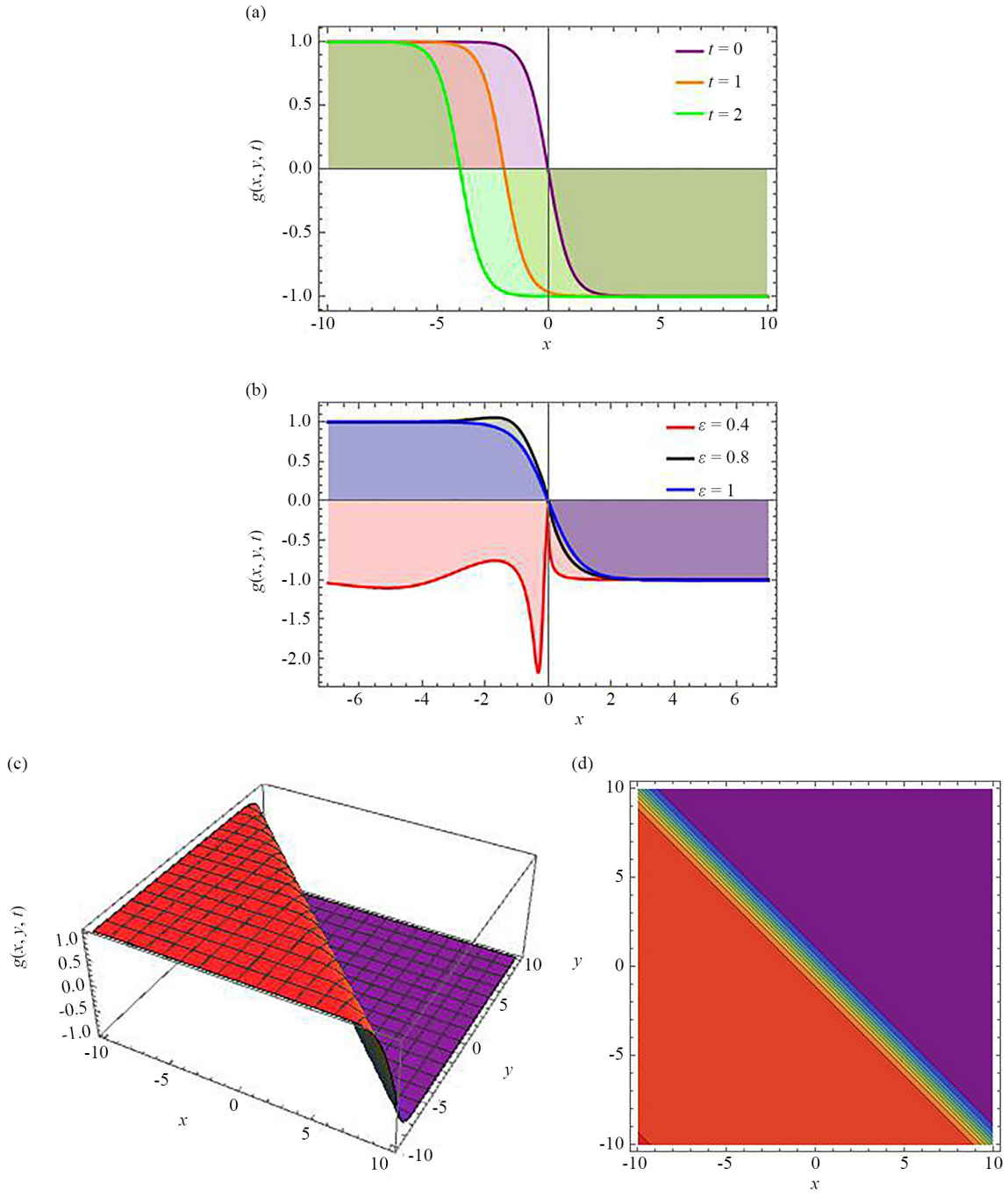

Figure 1. Graphical representation of $g(x,\ y,\ t)$ appearance in Eq. (31) for $\Delta = -1$ and $\rho = 1$. (a) demonstrates the kink-like 2-D graph when $-10 < x < 10$ for $\varepsilon = 1$ and $y = 0$ at different values of t. The purple color represents the graph at $t = 0$, the orange color denotes the graph at $t = 1$, while the green color demonstrates the graph at $t = 2$. We can observe that the wave solution is time-dependent because the phase of the wave solution is shifted with time. (b) displays a 2-dimensional graph if $-7 < x < 7$ for $t = 0$ and $y = 0$ at different values of ε. The red color shows the graph at $\varepsilon = 0.4$, black color denotes the graph at $\varepsilon = 0.8$, and blue color represents the graph at $\varepsilon = 1$. We can observe that the wave solution is ε dependent because the width of the graph changes with the change in the value of ε. (c) demonstrates the 3D plot when $-10 < x < 10$ and $-10 < y < 10$ at $\varepsilon = 1$ with $t = 0$. This shows that the wave solution has a symmetric property because the wave solution has a sharp transition in both x-direction and the y-direction. (d) indicates a contour graph when $-10 < x < 10$ and $-10 < y < 10$ at $\varepsilon = 1$ along with $t = 0$. Kink-like solution has many applications in different fields such as physics, materials science, biology, cosmology, etc

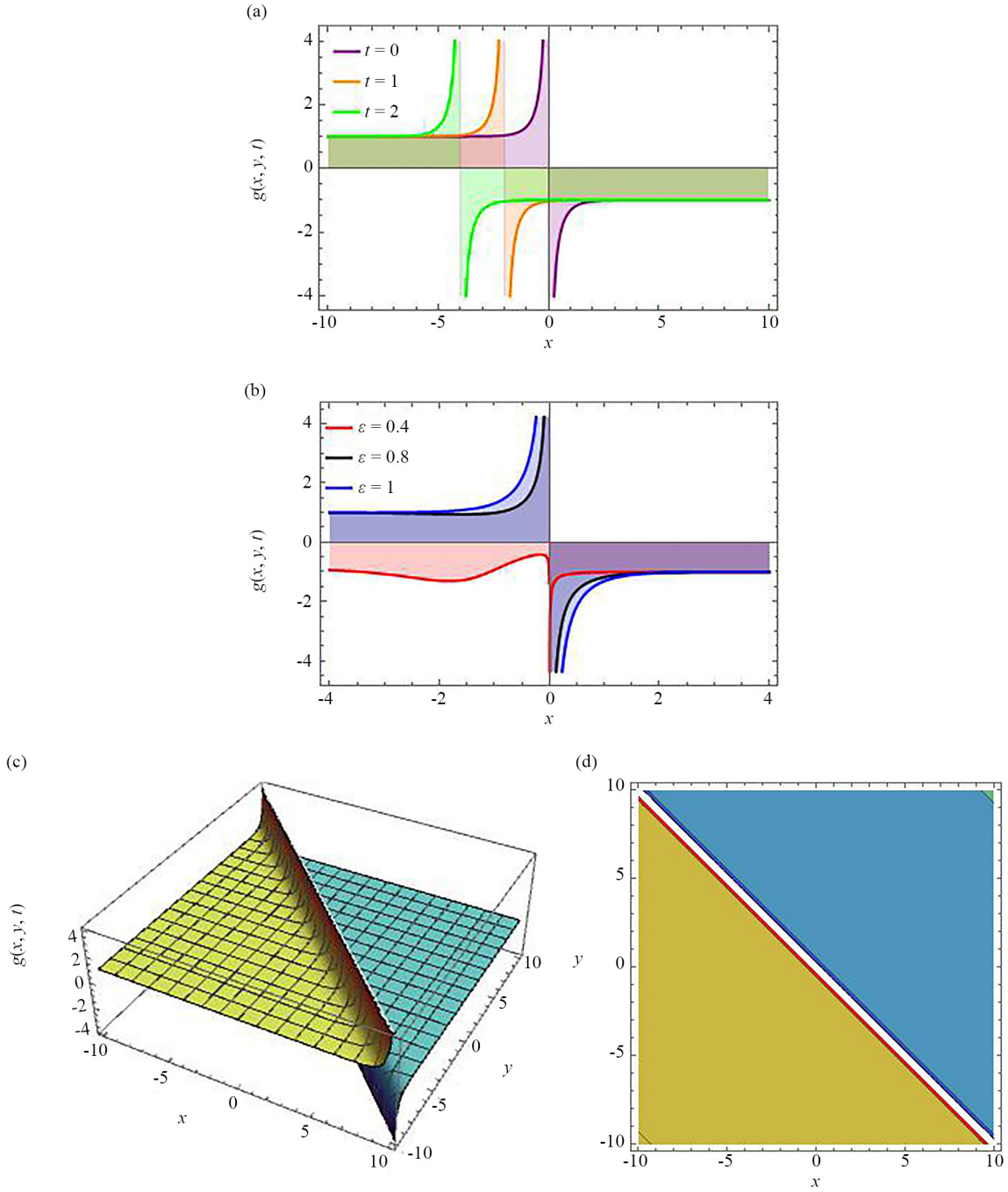

Figure 2. Graphical representation of $g(x,\ y,\ t)$ appearance in Eq. (32) for $\Delta = -1$ and $\rho = 1$. (a) demonstrates the singular wave 2-D graph when $-10 < x < 10$ for $\varepsilon = 1$ and $y = 0$ at different values of t. The purple color represents the graph at $t = 0$, the orange color shows the graph at $t = 1$, while the green color denotes the graph at $t = 2$. We can observe that the wave solution is time-dependent because the phase of the wave solution is shifted with time. (b) displays a 2-dimensional graph if $-4 < x < 4$ for $t = 0$ and $y = 0$ at different values of ε. The red color shows the graph at $\varepsilon = 0.4$, black color denotes the graph at $\varepsilon = 0.8$, and blue color represents the graph at $\varepsilon = 1$. We can observe that the wave solution is ε dependent because the width of the graph changes with the change in the value of ε. (c) demonstrates the 3D plot when $-10 < x < 10$ and $-10 < y < 10$ at $\varepsilon = 1$ with $t = 0$. This shows that the wave solution has a symmetric property because the wave solution has a sharp transition in both the x-direction and y-direction. (d) indicates a contour graph when $-10 < x < 10$ and $-10 < y < 10$ at $\varepsilon = 1$ along with $t = 0$. Singular wave solution has many applications in different fields such as optics, materials science, biology, ecology, etc

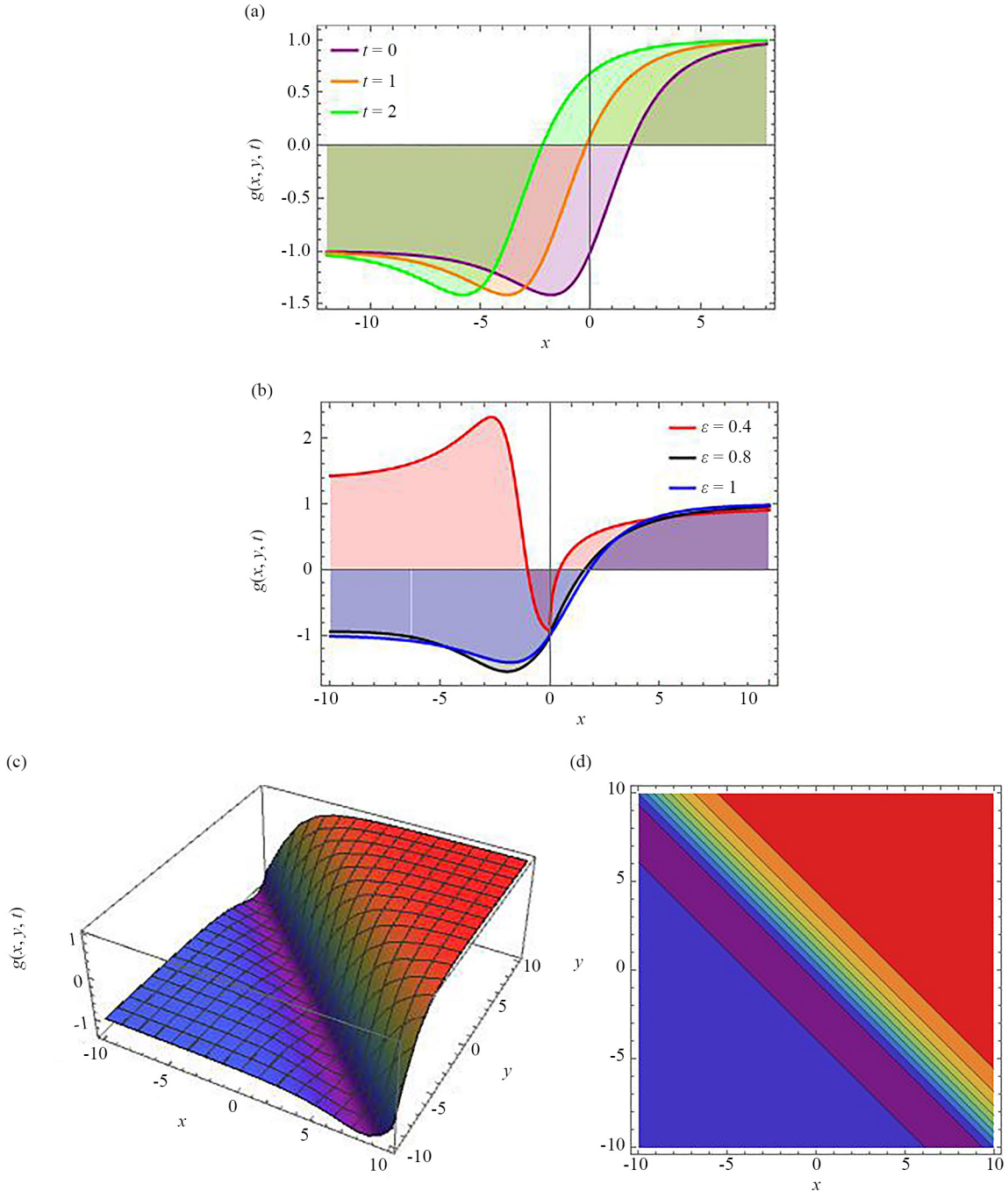

Figure 3. Graphical representation of $g(x,\ y,\ t)$ appearance in Eq. (33) for $\Delta = -0.06$ and $\rho = 1$. (a) demonstrates the soliton-like 2-D graph when $-12 < x < 8$ for $\varepsilon = 1$ and $y = 0$ at different values of t. The purple color represents the graph at $t = 0$, the orange color shows the graph at $t = 1$, while the green color denotes the graph at $t = 2$. We can observe that the wave solution is time-dependent because the phase of the wave solution is shifted with time. (b) displays a 2-dimensional graph if $-10 < x < 10$ for $t = 0$ and $y = 0$ at different values of ε. The red color shows the graph at $\varepsilon = 0.4$, black color denotes the graph at $\varepsilon = 0.8$, and blue color represents the graph at $\varepsilon = 1$. We can observe that the wave solution is ε dependent because the width of the graph changes with the change in the value of ε. (c) demonstrates the 3D plot when $-10 < x < 10$ and $-10 < y < 10$ at $\varepsilon = 1$ with $t = 0$. This shows that the wave solution has a symmetric property because the wave solution has a sharp transition in both the x-direction and the y-direction. (d) indicates a contour graph when $-10 < x < 10$ and $-10 < y < 10$ at $\varepsilon = 1$ along with $t = 0$. Soliton-like solution has many applications in different fields such as communication systems, nonlinear dynamics, biology, optical fibers, water waves, quantum field theory, etc

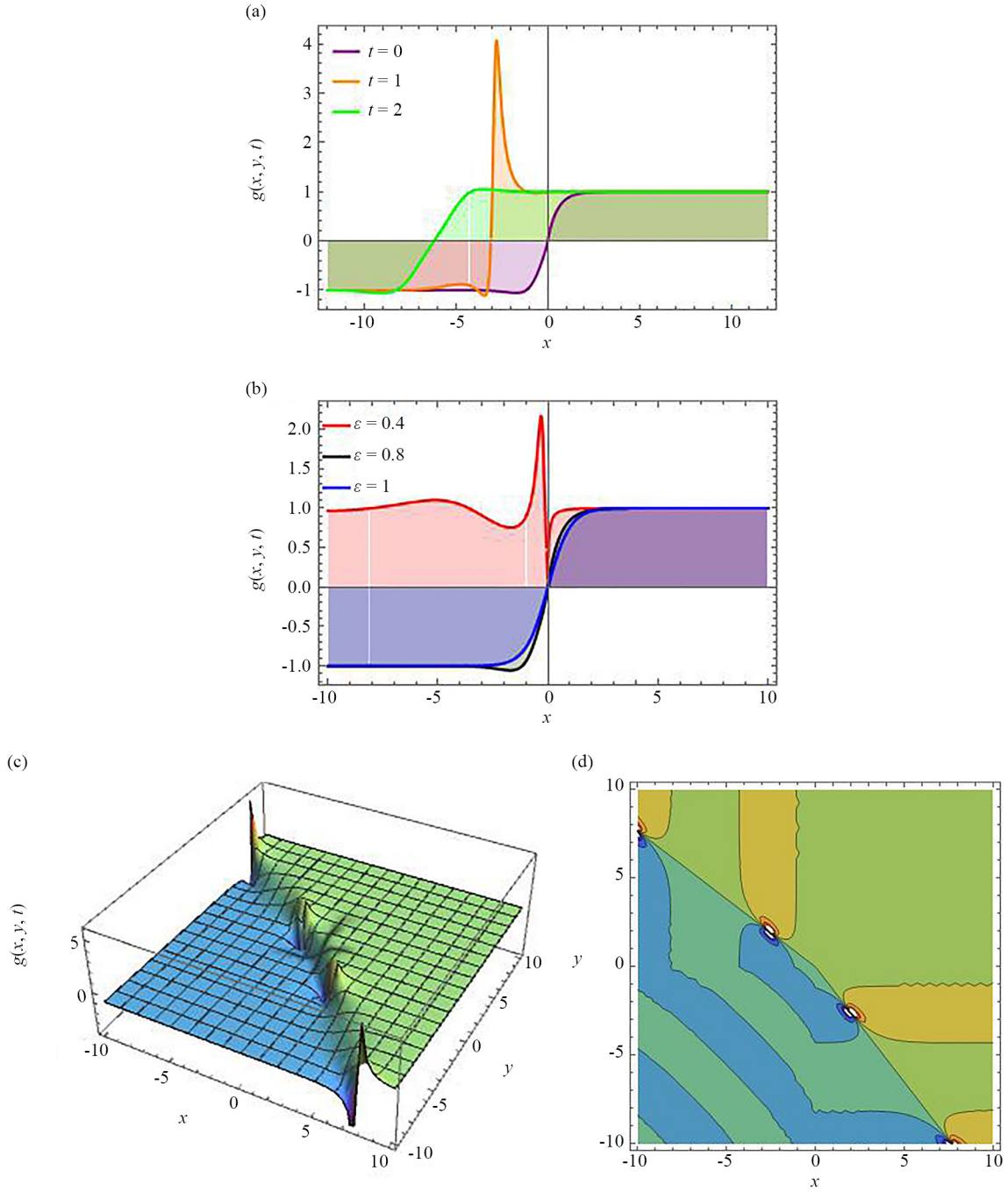

Figure 4. Graphical representation of $g(x, y, t)$ appearance in Eq. (34) for $\Delta = -1$ and $\rho = 1$. (a) demonstrates the complexiton solution 2-D graph when $-12 < x < 12$ for $\varepsilon = 1$ and $y = 0$ at different values of t. The purple color represents the graph at $t = 0$, the orange color denotes the graph at $t = 1$, while the green color shows the graph at $t = 2$. We can observe that the wave solution is time-dependent because the phase of the wave solution is shifted with time. (b) displays a 2-dimensional graph if $-10 < x < 10$ for $t = 0$ and $y = 0$ at different values of ε. The red color shows the graph at $\varepsilon = 0.4$, black color denotes the graph at $\varepsilon = 0.8$, and blue color represents the graph at $\varepsilon = 1$. We can observe that the wave solution is ε dependent because the width of the graph changes with the change in the value of ε. (c) demonstrates the 3D plot when $-10 < x < 10$ and $-10 < y < 10$ at $\varepsilon = 0.8$ with $t = 0$. This shows that the wave solution has a symmetric property because the wave solution has a sharp transition in both the x-direction and the y-direction. (d) indicates a contour graph when $-10 < x < 10$ and $-10 < y < 10$ at $\varepsilon = 0.8$ along with $t = 0$. Complexiton solution has many applications in different fields such as nonlinear optics, quantum mechanics, fluid dynamics, etc

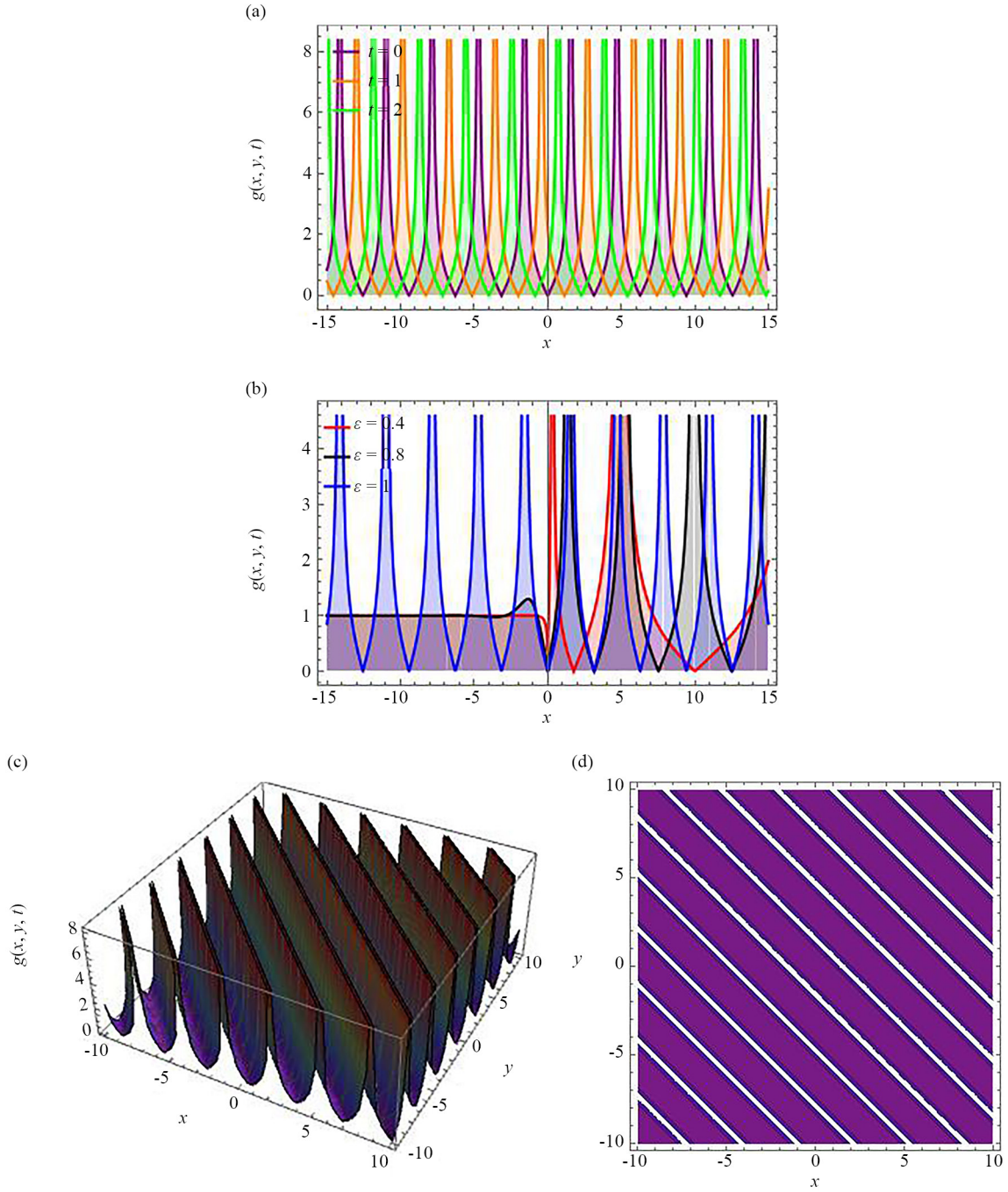

Figure 5. Graphical representation of $g(x, y, t)$ appearance in Eq. (36) for $\Delta = 1$ and $\rho = 1$. (a) demonstrates the 2-D graph of periodic solution when $-15 < x < 15$ for $\varepsilon = 1$ and $y = 0$ at different values of t. The purple color represents the graph at $t = 0$, the orange color shows the graph at $t = 1$, while the green color denotes the graph at $t = 2$. We can observe that the wave solution is time-dependent because the phase of the wave solution is shifted along with time. (b) displays a 2-dimensional graph if $-15 < x < 15$ for $t = 0$ and $y = 0$ at different values of ε. The red color shows the graph at $\varepsilon = 0.4$, black color denotes the graph at $\varepsilon = 0.8$, and blue color represents the graph at $\varepsilon = 1$. We can observe that the wave solution is ε dependent because the width of the graph changes with the change in the value of ε. (c) demonstrates the 3D plot when $-10 < x < 10$ and $-10 < y < 10$ at $\varepsilon = 1$ with $t = 0$. This shows that the wave solution has a symmetric property because the wave solution has a sharp transition in both the x-direction and the y-direction. (d) indicates a contour graph when $-10 < x < 10$ and $-10 < y < 10$ at $\varepsilon = 1$ along with $t = 0$. Periodic wave solution has various applications in many areas such as economics, biology, engineering, physics, etc

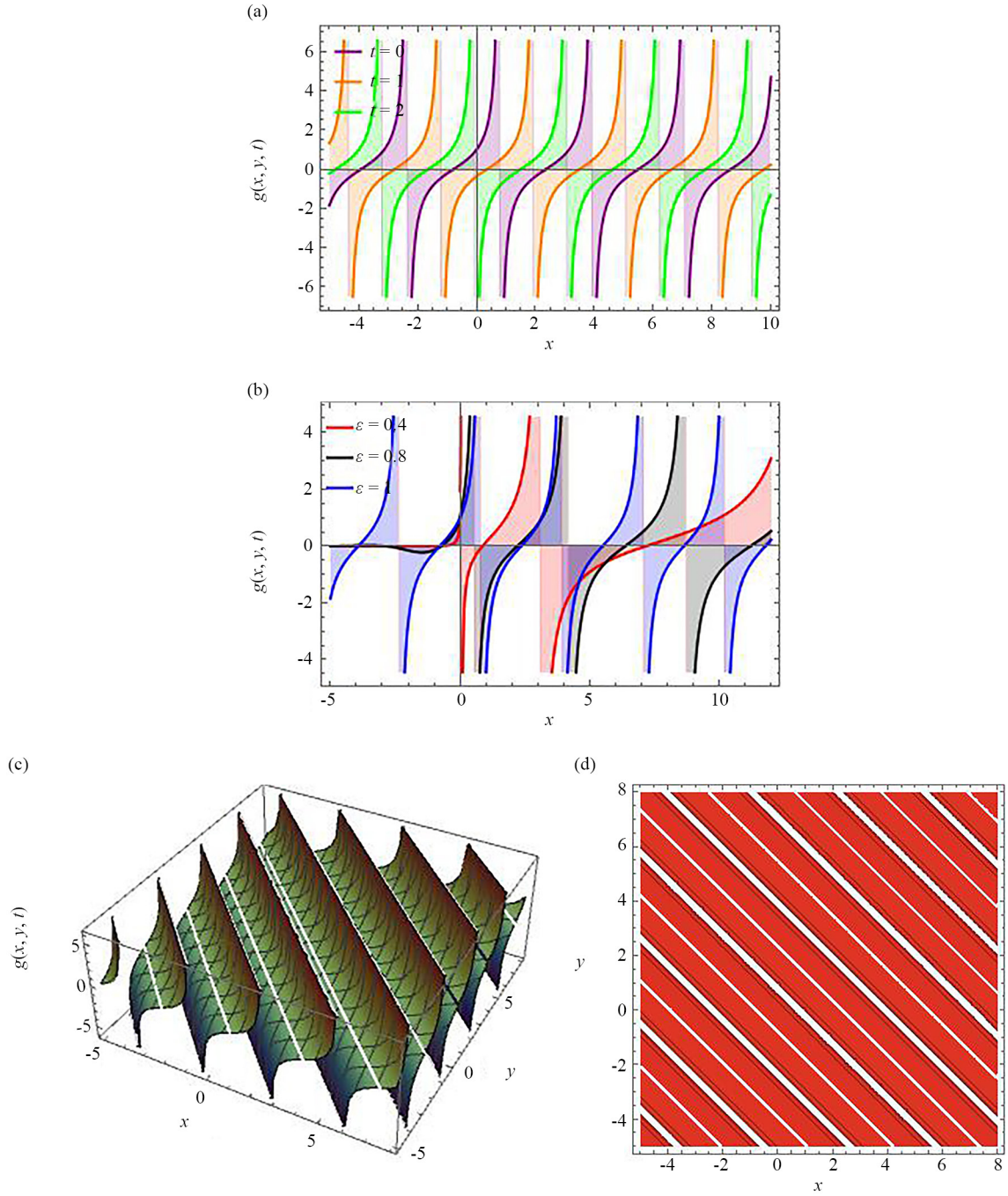

Figure 6. Graphical representation of $g(x, y, t)$ appearance in Eq. (38) for $\Delta = 1$ and $\rho = 1$. (a) demonstrates the 2-D graph of dark soliton solution when $-5 < x < 10$ for $\varepsilon = 1$ and $y = 0$ at different values of t. The purple color represents the graph at $t = 0$, the orange color denotes the graph at $t = 1$, while the green color shows the graph at $t = 2$. We can observe that the wave solution is time-dependent because the phase of the wave solution is shifted with time. (b) displays a 2-dimensional graph if $-5 < x < 12$ for $t = 0$ and $y = 0$ at different values of ε. The red color shows the graph at $\varepsilon = 0.4$, black color denotes the graph at $\varepsilon = 0.8$, and blue color represents the graph at $\varepsilon = 1$. We can observe that the wave solution is ε dependent because the width of the graph changes with the change in the value of ε. (c) demonstrates the 3D plot when $-5 < x < 8$ and $-5 < y < 8$ at $\varepsilon = 1$ with $t = 0$. This shows that the wave solution has a symmetric property because the wave solution has a wave-like structure in both the x-direction and the y-direction. (d) indicates a contour graph when $-5 < x < 8$ and $-5 < y < 8$ at $\varepsilon = 1$ along with $t = 0$. Dark soliton solution has various applications in many areas such as nonlinear optics, fluid dynamics, physics, etc

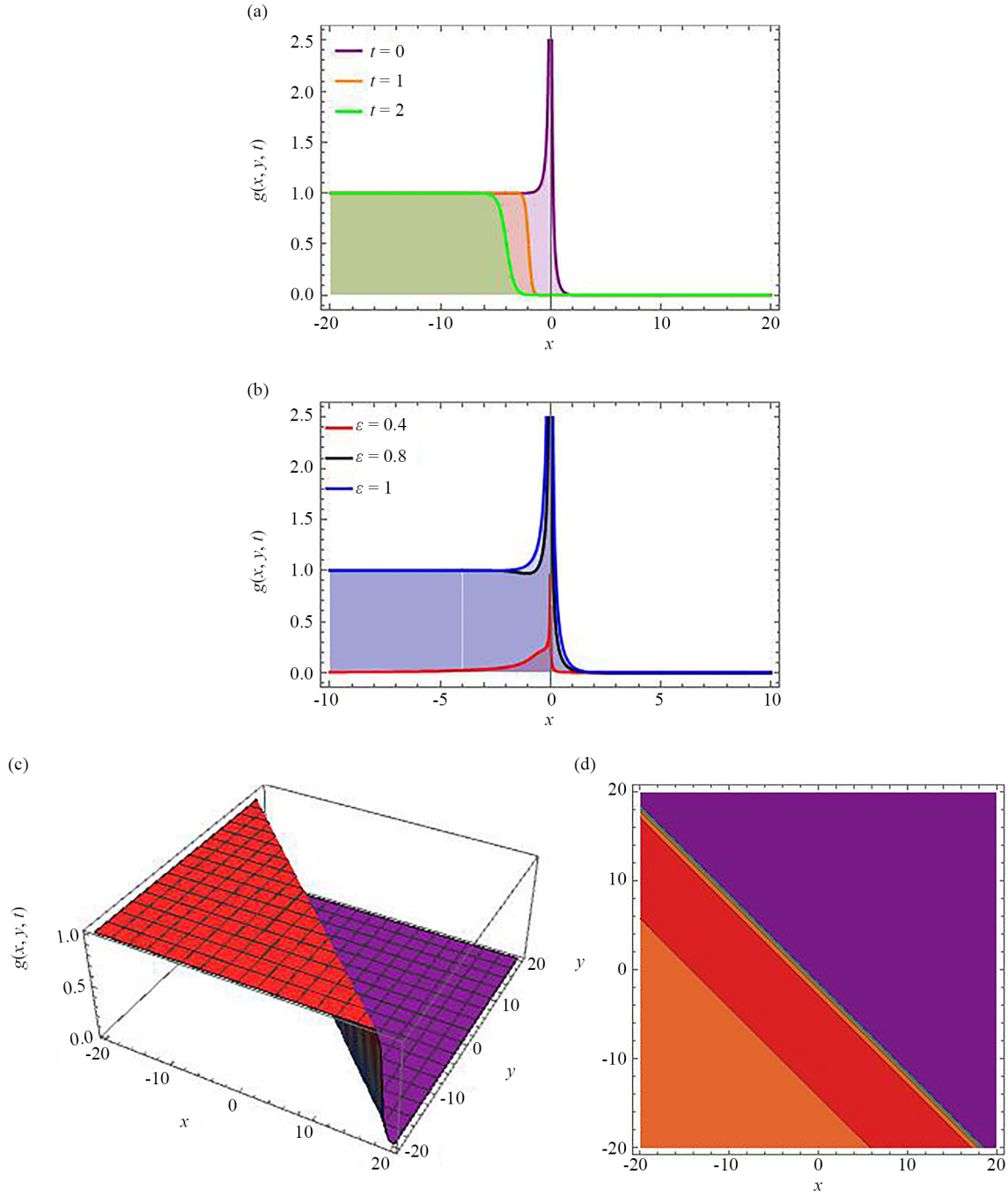

Figure 7. Graphical representation of $g(x, y, t)$ appearance in Eq. (40) for $\Delta = -2$ and $\rho = 1$. (a) demonstrates the 2-D graph of topological soliton solution when $-20 < x < 20$ for $\varepsilon = 1$ and $y = 0$ at different values of t. The purple color represents the graph at $t = 0$, the orange color shows the graph at $t = 1$, while the green color denotes the graph at $t = 2$. We can observe that the wave solution is time-dependent because the phase of the wave solution is shifted with time. (b) displays a 2-dimensional graph if $-10 < x < 10$ for $t = 0$ and $y = 0$ at different values of ε. The red color shows the graph at $\varepsilon = 0.4$, black color denotes the graph at $\varepsilon = 0.8$, and blue color represents the graph at $\varepsilon = 1$. We can observe that the wave solution is ε dependent because the width of the graph changes with the change in the value of ε. (c) demonstrates the 3D plot when $-20 < x < 20$ and $-20 < y < 20$ at $\varepsilon = 1$ with $t = 1$. This shows that the wave solution has a symmetric property because the wave solution has a sharp transition in both the x-direction and the y-direction. (d) indicates a contour graph when $-20 < x < 20$ and $-20 < y < 20$ at $\varepsilon = 1$ along with $t = 1$. Topological soliton solution has many applications in different areas like nonlinear optics, condensed matter physics, field theory, etc

5. Stability analysis

It has much significance in many fields of science and engineering. Stability analysis is done by applying the characteristics of the Hamiltonian function is checked for some achieved results to find the stability of concerning equation. In the literature, the stability analysis of various equations has been explained [26–28].

Here, we discuss the stability of the solutions. For this purpose, we define the Hamiltonian function as,

$$\mathscr{S} = \frac{1}{2}\int_{-\infty}^{\infty} g^2\, dx, \tag{52}$$

for dissipative terms $g^3 - g$, above Eq. (52) becomes:

$$\mathscr{S} = \frac{1}{2}\int_{-\infty}^{\infty} g^2\, dx + \int_{-\infty}^{\infty} (\frac{g^4}{4} - \frac{g^2}{2})\, dx \tag{53}$$

or

$$\mathscr{S} = \frac{1}{4}\int_{-\infty}^{\infty} g^4\, dx, \tag{54}$$

where, momentum factor is denoted by $\mathscr{S}$. We present prerequisites for a stable soliton.

$$\frac{\partial \mathscr{S}}{\partial \omega} > 0, \tag{55}$$

here ω is a wave speed, using Eq. (31) into Eq. (54) provides;

$$\mathscr{S} = \frac{1}{4}\int_{-10}^{10} (\frac{1}{\sqrt{-\Delta}}(\sqrt{-\Delta}\tanh(\sqrt{-\Delta}\,(x+y+\omega t))))^4 dx, \tag{56}$$

by using the criterion given in Eq. (55), we obtain

$$\begin{aligned} &\frac{1}{12}(-t(\sec^2(\sqrt{\Delta}(2t+y-10)) - 4)\sec^2(\sqrt{\Delta}(2t+y-10)) + t\sec^2(\sqrt{\Delta}(2t+y+10)) \\ &(\sec^2(\sqrt{\Delta}(2t+y+10)) - 4) + 2t\tan^2(\sqrt{\Delta}(2t+y-10))\sec^2(\sqrt{\Delta}(2t+y-10)) \\ &- 2t\tan^2(\sqrt{\Delta}(2t+y+10))\sec^2(\sqrt{\Delta}(2t+y+10))) > 0. \end{aligned} \tag{57}$$

By putting the values: $\Delta = 1,\ y = 0$, and $t = 1$ in the above expression (57), we obtain $0.00341 > 0$.

Hence, Eq. (31) satisfies the above-mentioned condition, so the solution mentioned in Eq. (31) is stable. Similarly, we can check the stability of the remaining solutions one by one.

6. Modulation instability

Modulation instability is a phenomenon where a small perturbation in a continuous wave grows exponentially, leading to the breakdown of the wave's stability. This instability can occur in many nonlinear systems, including optics, fluids, plasmas, etc. By performing modulation instability analysis, researchers can gain insights into the stability and nonlinear behavior of the system, which is helpful for understanding the complex phenomenon easily.

Assuming a solution of the (2 + 1)-dimensional Fisher-Kolmogorov-Petrovskii-Piskunov model is represented in [29, 30].

$$g(x,\, y,\, t) = \left(\sqrt{\tau} + G(x,\, y,\, t)\right) \mathrm{e}^{\iota \tau t}, \tag{58}$$

here τ denotes an arbitrary real constant, and $G(x,\, y,\, t)$ is a complex-valued function of $x,\, y$, and t. Eq. (58) represents the periodic complex backgrounds, which can be used to study the emergence of patterns in reaction-diffusion systems, including stripes, spots, or more complex geometries. It can provide insights into the mechanisms underlying pattern formation in reaction-diffusion systems.

Putting the Eq. (58) into Eq. (1), we obtain an equation for G by linearity given as:

$$\iota \tau G + G_t - G_x + \nu G_{xx} + 2\nu G_{xy} - G_y + \nu G_{yy} - G + \iota \tau^{3/2} - \sqrt{\tau} = 0. \tag{59}$$

Now consider a new transformation given as:

$$G(x,\, y,\, t) = G_1 \mathrm{e}^{\iota(\rho x + \theta y - t\lambda)} + G_2 \mathrm{e}^{-\iota(\rho x + \theta y - t\lambda)}, \tag{60}$$

here ρ, and θ are real disturbance wave numbers, λ represents a frequency while G_1 and G_2 are the coefficients of linear combination. By using Eq. (60) in the Eq. (59), we get homogeneous equations given as:

$$\begin{aligned} G_1 \left(-\theta^2 \nu - \theta \iota - 2\theta \nu \rho - \iota \lambda - \iota \rho + \iota \tau - \nu \rho^2 - 1\right) = 0, \\ G_2 \left(-\theta^2 \nu + \theta \iota - 2\theta \nu \rho + \iota \lambda + \iota \rho + \iota \tau - \nu \rho^2 - 1\right) = 0. \end{aligned} \tag{61}$$

Determinant of system of Eq. (61) is taking to 0: we get the following relation:

$$(-\theta^2 \nu - \theta \iota - 2\theta \nu \rho - \iota \lambda - \iota \rho + \iota \tau - \nu \rho^2 - 1)(-\theta^2 \nu + \theta \iota - 2\theta \nu \rho + \iota \lambda + \iota \rho + \iota \tau - \nu \rho^2 - 1) = 0. \tag{62}$$

Assuming Eq. (62), we can discuss types of Modulation Instability (MI) of Eq. (1) given as.

$$\lambda = -\rho - \theta \pm \sqrt{-\theta^4 \nu^2 - 4\theta^3 \nu^2 \rho - 6\theta^2 \nu^2 \rho^2 - 2\theta^2 \nu - 4\theta \nu^2 \rho^3 - 4\theta \nu \rho - \nu^2 \rho^4 - 2\nu \rho^2 + \tau^2 - 1}. \tag{63}$$

A steady-state stable solution is found by Eq. (63).

If λ has an imaginary part, then the steady-state solution is not stable because the perturbation increases exponentially.

If λ is not an imaginary part, then the steady-state solution is stable because the perturbation is small. Hence, MI of Eq. (63) occur if

$$-\theta^4\nu^2 - 4\theta^3\nu^2\rho - 6\theta^2\nu^2\rho^2 - 2\theta^2\nu - 4\theta\nu^2\rho^3 - 4\theta\nu\rho - \nu^2\rho^4 - 2\nu\rho^2 + \tau^2 - 1 < 0. \tag{64}$$

Therefore, we obtain the MI gain spectrum given as;

$$\begin{aligned} G(\rho) &= 2Im(\lambda) \\ &= 2Im\left(-\rho - \theta \pm \sqrt{-\theta^4\nu^2 - 4\theta^3\nu^2\rho - 6\theta^2\nu^2\rho^2 - 2\theta^2\nu - 4\theta\nu^2\rho^3 - 4\theta\nu\rho - \nu^2\rho^4 - 2\nu\rho^2 + \tau^2 - 1}\right). \end{aligned} \tag{65}$$

7. Asymptotic behavior

Asymptotic analysis has many advantages. Instantly, this analysis helps simplify complex mathematical models by focusing on the dominant behavior as a parameter approaches a limiting value. This analysis provides valuable insights into the behavior of functions or systems. Asymptotic analysis can be used for a wide range of mathematical and physical models, including differential equations, integrals, and algebraic equations, etc. Asymptotic analysis is applied to study various physical phenomena, such as fluid dynamics, quantum mechanics, and optics. Now, authors demonstrate the asymptotic behaviors of the obtained solutions. We describe the x-asymptotic, y-asymptotic, and t-asymptotic with the use of 2-D graphs.

8. Conclusion

It is concluded that the MSE scheme was utilized for the concerning model in obtaining distinct kinds of exact wave results for the truncated M-fractional Fisher-Kolmogorov-Petrovskii-Piskunov model equation. The gained results are demonstrated by 2-D, 3-D, and contour graphs in Figures 1-7. The gained solutions were not studied earlier. The benefit of the used new definition of derivative is that it provides solutions closer to numerical solutions. The obtained solutions are helpful in ecology, gene mutation, combustion theory, phase transition, etc. The stability of a governing system is checked by applying stability analysis. By using the modulation instability analysis, steady-state solutions are obtained. The modulation instability analysis is also explained through Figure 8. Moreover, asymptotic analysis is explained for the obtained solutions with the use of 2D graphs in Figures 9-13. At the end, this research is helpful in the further development of the governing model.

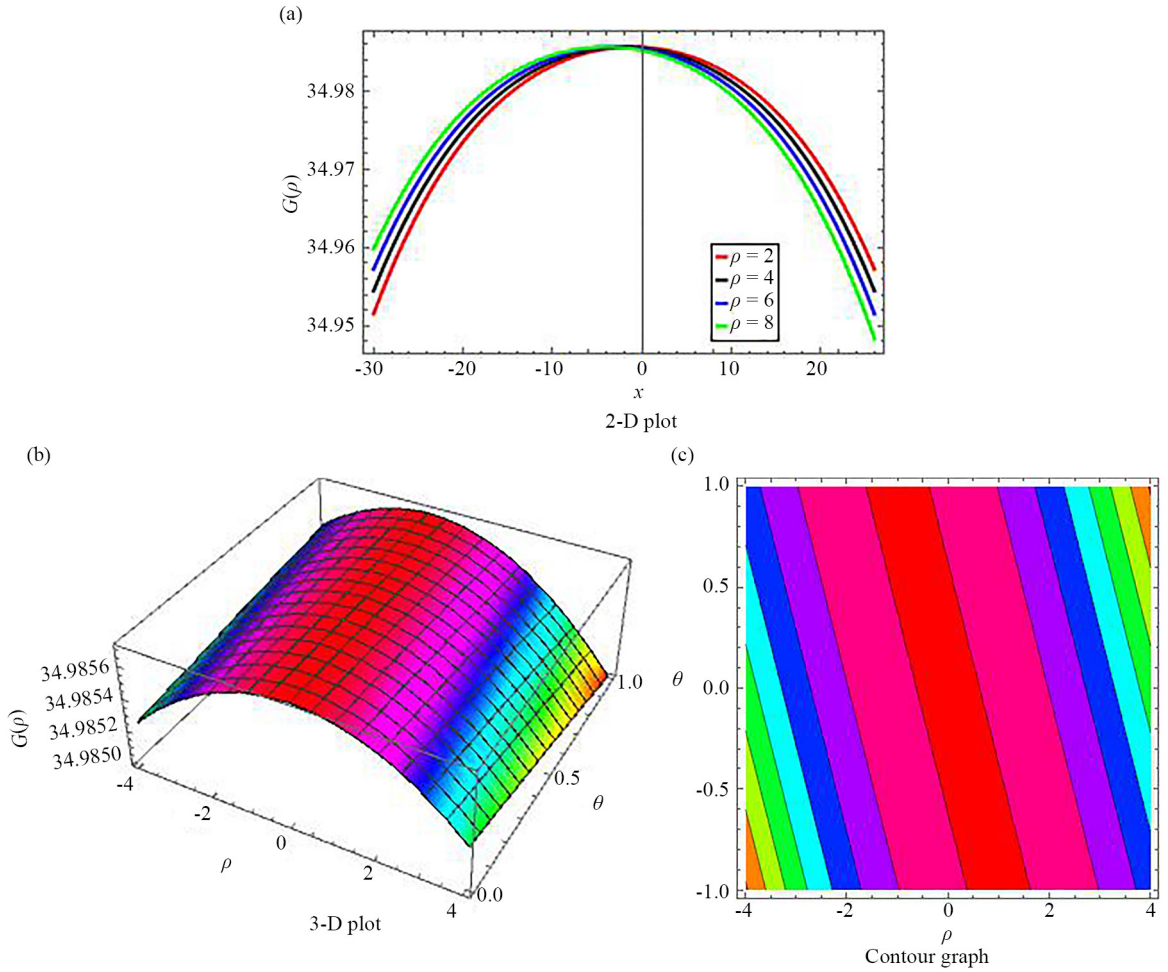

Figure 8. Gain spectrum of modulation instability for $\rho = 2,\ 4,\ 6,\ 8$ and $\tau = 35$ and $\nu = 0.001$ in Eq. (65). (a) represents the 2D graph; the red curve is for $\rho = 2$, the purple curve is for $\rho = 4$, the blue curve is for $\rho = 6$, and the green curve is for $\rho = 8$. (b) shows the 3D graph when $\theta \in (0,\ 1)$ and $\rho \in (-4,\ 4)$. (c) denotes the contour graph when $\theta \in (0,\ 1)$ and $\rho \in (-4,\ 4)$. The gain spectrum of modulation instability can inform the design of systems such as optical fibers or lasers to optimize their performance and stability. By modulation instability gain spectrum, researchers can gain insights into the stability and nonlinear behavior of the system, which is helpful for understanding the complex phenomenon easily

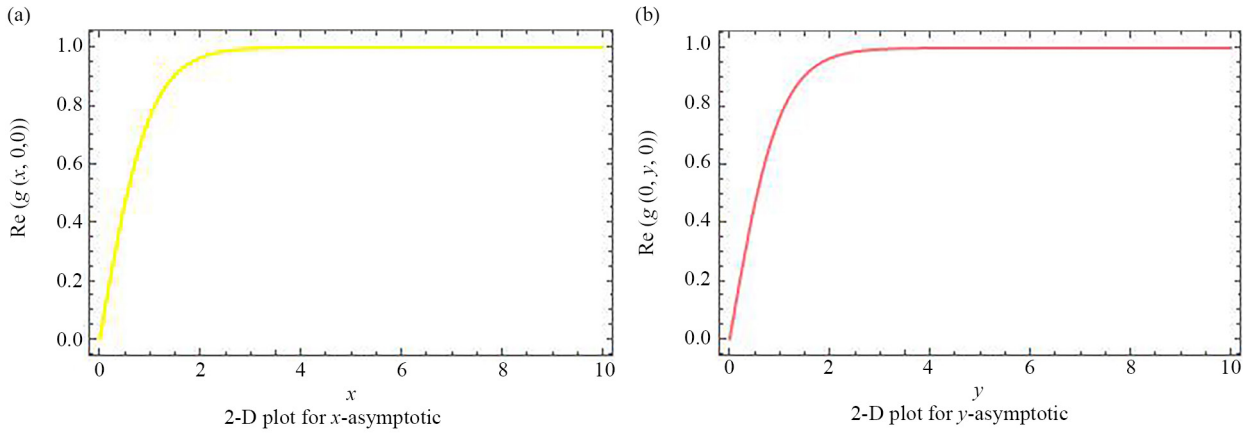

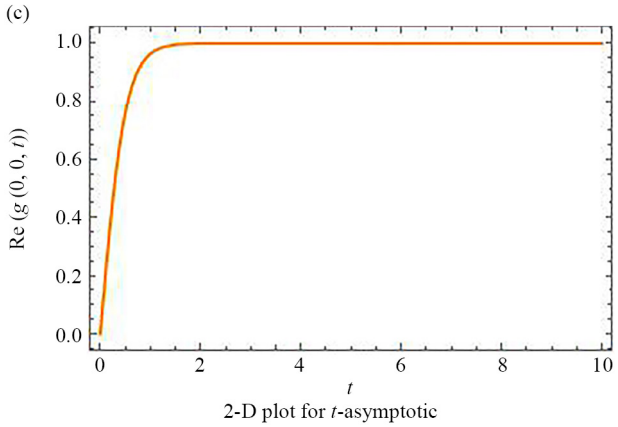

Figure 9. Asymptotic behavior of the solution given in Eq. (31) for $\Delta = -1$, $\varepsilon = 1$, and $\rho = 1$. (a) represents the x-asymptotic when $y = 0$ and $t = 0$. (b) represents the y-asymptotic when $x = 0$ and $t = 0$. (c) represents the t-asymptotic when $x = 0$ and $y = 0$. The real part helps isolate the measurable or observable component of a potentially complex-valued function. The shape suggests a localized structure, often properties of solitons. It's localized and smooth, which suggests stability: the solution might preserve this shape while moving

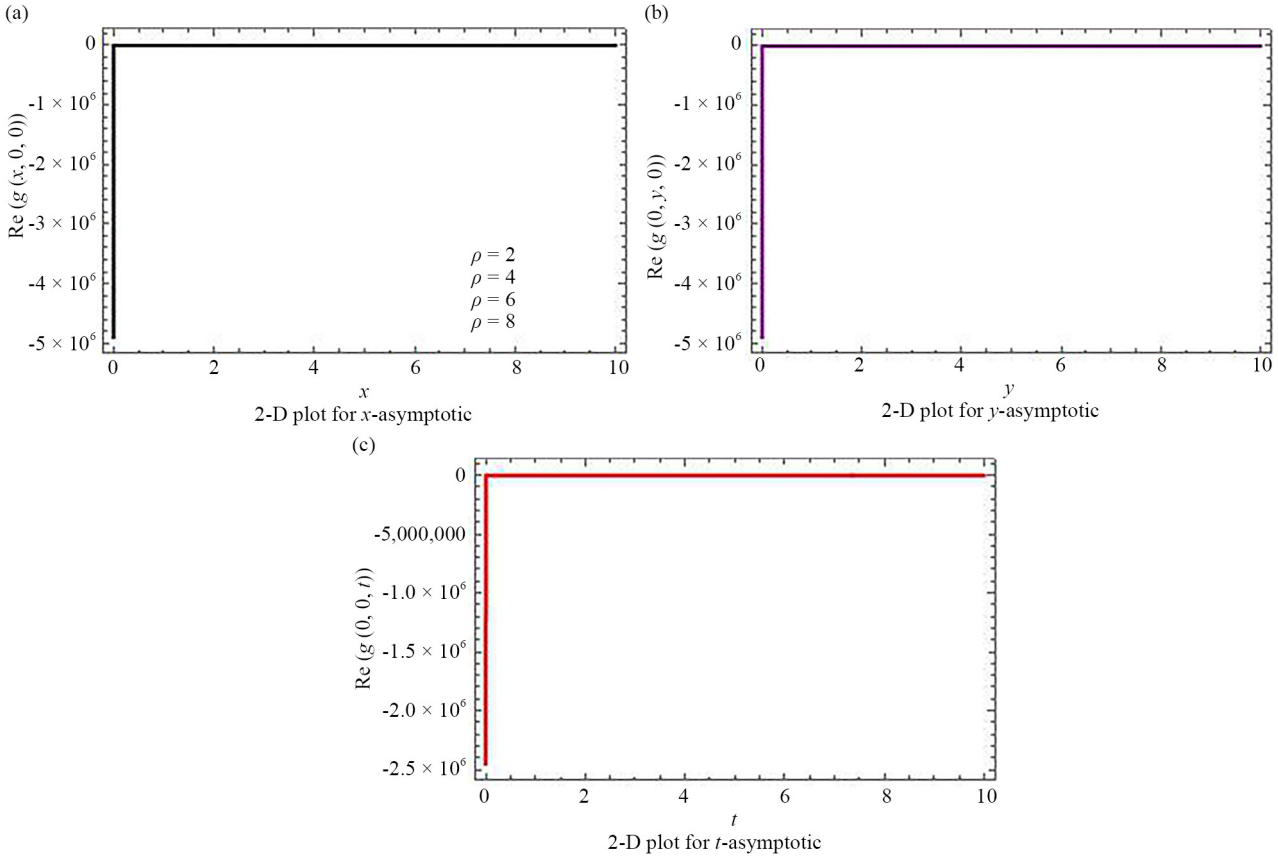

Figure 10. Asymptotic behavior of the solution given in Eq. (32) for $\Delta = -1$, $\varepsilon = 1$, and $\rho = 1$. (a) represents the x-asymptotic when $y = 0$ and $t = 0$. (b) represents the y-asymptotic when $x = 0$ and $t = 0$. (c) represents the t-asymptotic when $x = 0$ and $y = 0$. The graph shows the real part of a complex-valued function, and a deep negative value represents a localized or inverted energy packet. This graph represents the spatial profile of a wave or disturbance in a physical system

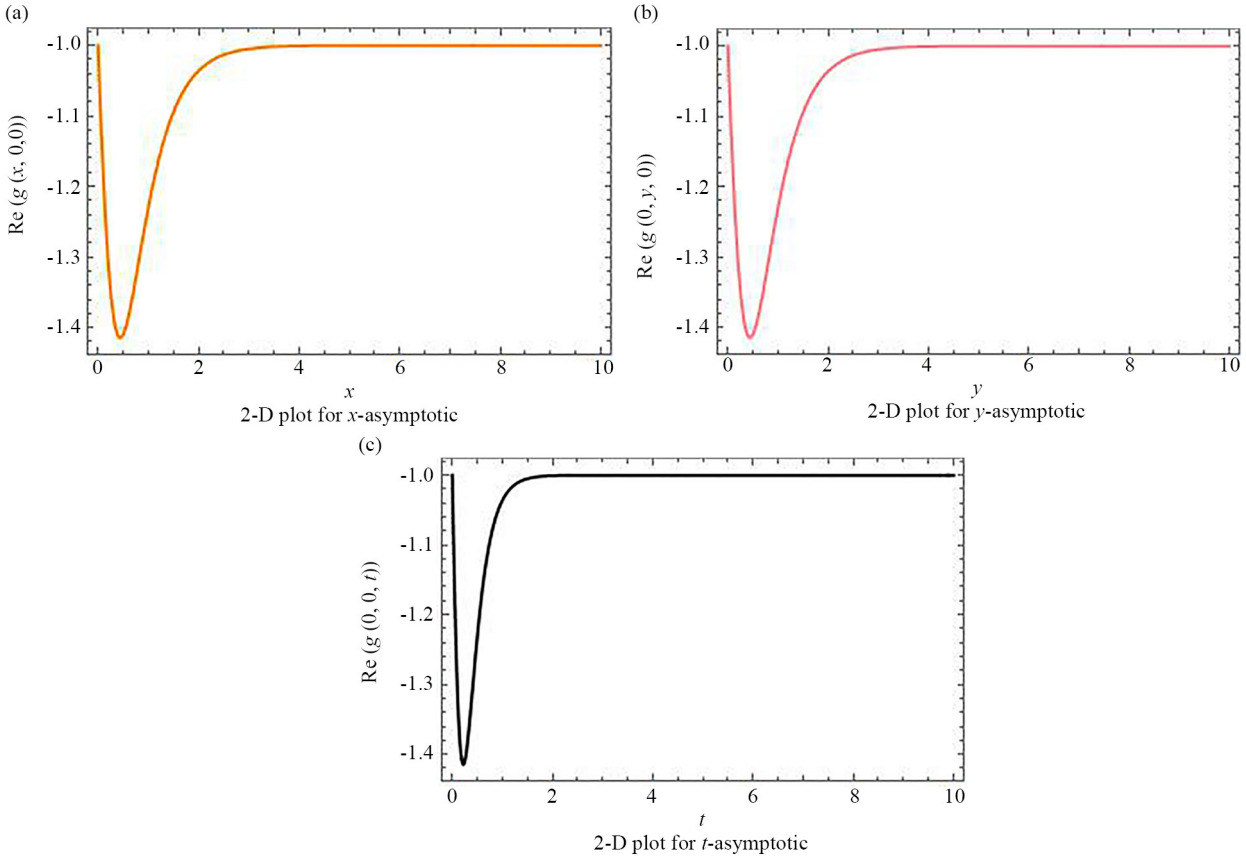

Figure 11. Asymptotic behavior of the solution given in Eq. (33) for $\Delta = -1$, $\varepsilon = 1$, and $\rho = 1$. (a) represents the x-asymptotic when $y = 0$ and $t = 0$. (b) represents the y-asymptotic when $x = 0$ and $t = 0$. (c) represents the t-asymptotic when $x = 0$ and $y = 0$. The graph shows the slowly varying function, suggesting it may show a background wave or low-energy state. The graph represents the stable, smooth, and negative-valued field distribution

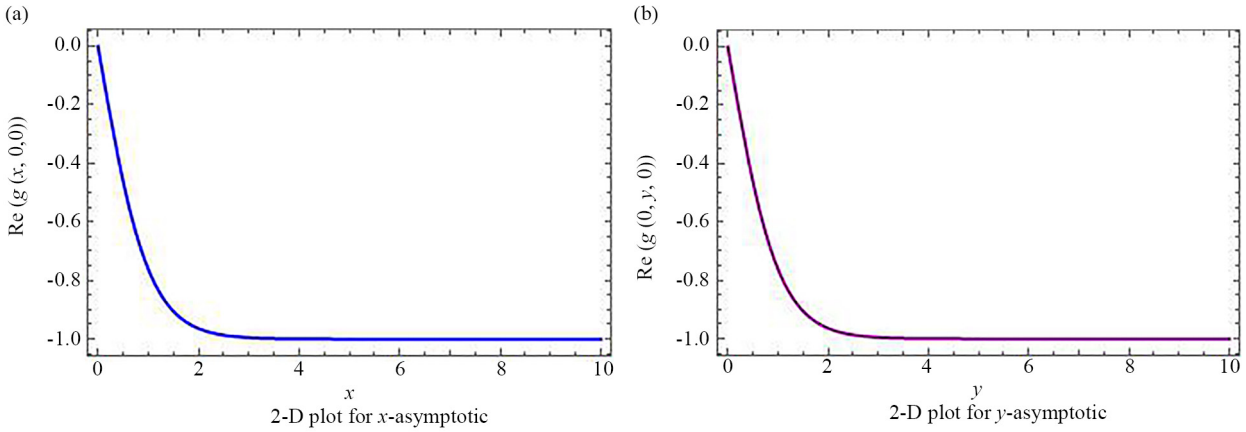

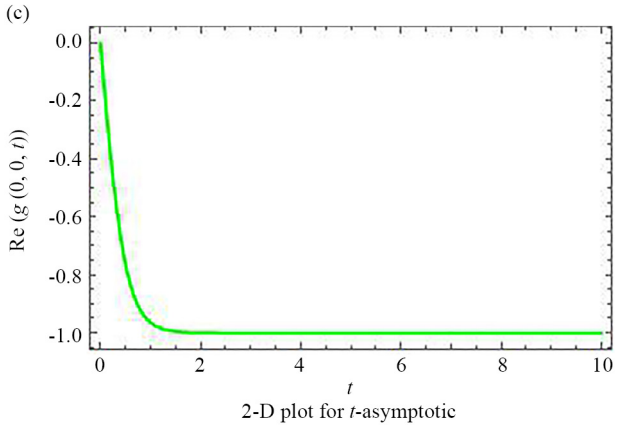

Figure 12. Asymptotic behavior of the solution given in Eq. (34) for $\Delta = -1$, $\varepsilon = 1$, and $\rho = 1$. (a) represents the x-asymptotic when $y = 0$ and $t = 0$. (b) represents the y-asymptotic when $x = 0$ and $t = 0$. (c) represents the t-asymptotic when $x = 0$ and $y = 0$. The graph shows the dissipation or dispersive decay. It is useful for understanding the transverse localization or stability of the function. We can observe that the function's behavior is far from the origin along each coordinate direction

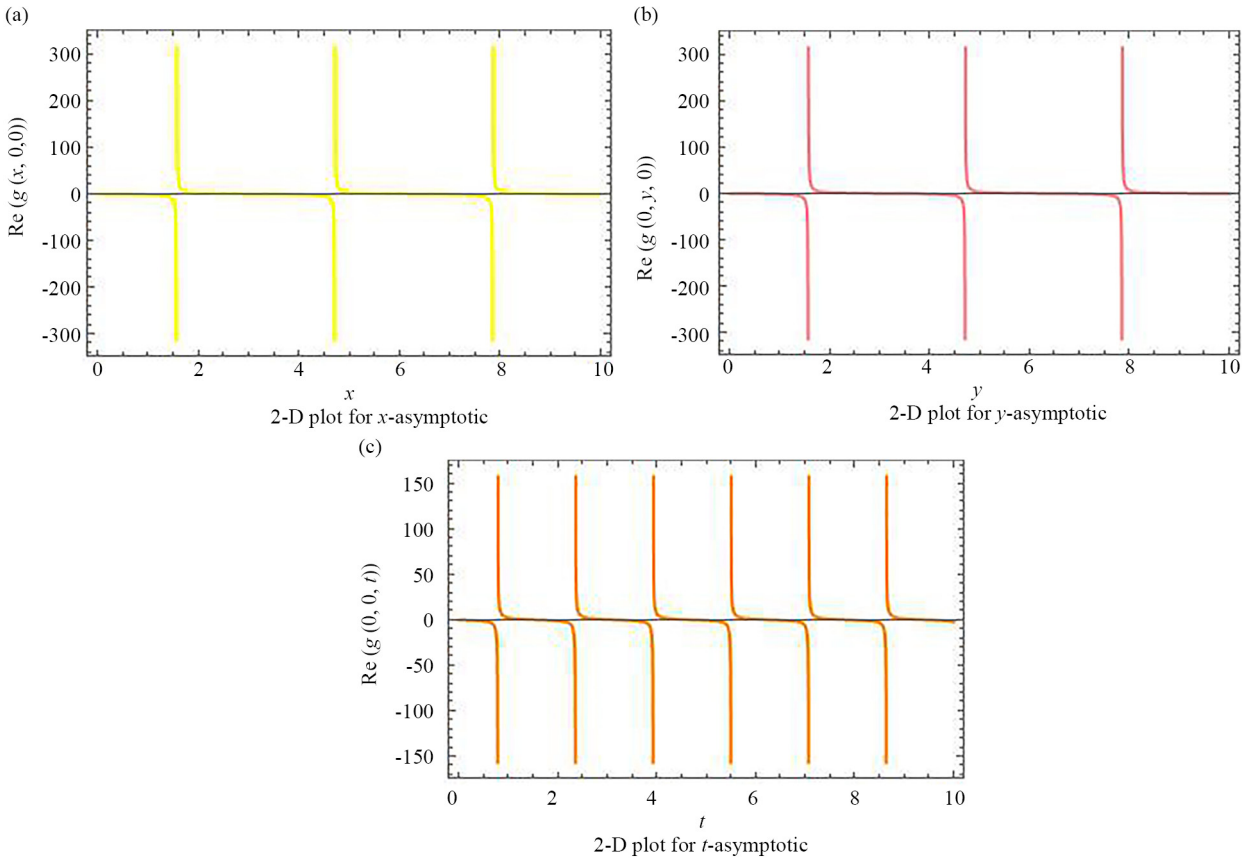

Figure 13. Asymptotic behavior of the solution given in Eq. (36) for $\Delta = 1$, $\varepsilon = 1$, and $\rho = 1$. (a) represents the x-asymptotic when $y = 0$ and $t = 0$. (b) represents the y-asymptotic when $x = 0$ and $t = 0$. (c) represents the t-asymptotic when $x = 0$ and $y = 0$. It is observed that the graph is not localized. It shows the temporal oscillation. Moreover, the graph indicates the non-decaying behavior

Data availability statement

The datasets used and/or analysed during the current study available from the corresponding author on reasonable request.

Acknowledgements

The authors gratefully acknowledge the support from the National Science and Technology Council (NSTC), Taiwan, under Project No. 113-2221-E-006-033-MY3. We also thank the Yushan Fellow Program (Project No. MOE-113-YSFEE-0005-001-P1) by the Ministry of Education (MOE), Taiwan, for the financial support.

Author's contributions

MR: Writing-review and editing, Conceptualization, Methodology, Project administration; DC: Funding, Conceptualization, Methodology; AZ: Conceptualization, Methodology, Formal Analysis, Supervision.

Conflict of interest

The authors declare no competing financial interest.

References

[1] Alaroud M, Aljarrah H, Alomari AK, Ishak A, Darus M. Explicit and approximate series solutions for nonlinear fractional wave-like differential equations with variable coefficients. *Partial Differential Equations in Applied Mathematics*. 2024; 10: 100680. Available from: https://doi.org/10.1016/j.padiff.2024.100680.

[2] Muhammad J, Rehman SU, Nasreen N, Bilal M, Younas U. Exploring the fractional effect to the optical wave propagation for the extended Kairat-II equation. *Nonlinear Dynamics*. 2025; 113(2): 1501-1512. Available from: https://doi.org/10.1007/s11071-024-10139-3.

[3] Thadee W, Phoosree S. New wave behaviors generated by simple equation method with Riccati equation of some fourth-order fractional water wave equations. *Journal of the Physical Society of Japan*. 2024; 93(1): 014002. Available from: https://doi.org/10.7566/JPSJ.93.014002.

[4] Ekici M. Travelling wave solutions for some time-fractional nonlinear differential equations. *Black Sea Journal of Engineering and Science*. 2024; 7(2): 246-253. Available from: https://doi.org/10.34248/bsengineering.1413250.

[5] Zhang J, Ou C, Wang Z, Vong S. An order reduction method for the nonlinear Caputo-Hadamard fractional diffusionwave model. *Communications on Applied Mathematics and Computation*. 2025; 7(1): 392-408. Available from: https://doi.org/10.1007/s42967-023-00295-5.

[6] Khater MM, Alabdali AM. Multiple novels and accurate traveling wave and numerical solutions of the (2 + 1) dimensional Fisher-Kolmogorov-Petrovskii-Piskunov equation. *Mathematics*. 2021; 9(12): 1440. Available from: https://doi.org/10.3390/math9121440.

[7] Oruç Ö. An efficient wavelet collocation method for nonlinear two-space dimensional Fisher-Kolmogorov-Petrovsky-Piscounov equation and two-space dimensional extended Fisher-Kolmogorov equation. *Engineering with Computers*. 2020; 36(3): 839-856. Available from: https://doi.org/10.1007/s00366-019-00734-z.

[8] Ullah I. Dynamics behaviours of N-kink solitons in conformable Fisher-Kolmogorov-Petrovskii-Piskunov equation. *Engineering Computations*. 2024; 41(10): 2404-2426. Available from: https://doi.org/10.1108/EC-04-2024-0358.

[9] Baladezaei MG, Gachpazan M, Foadian S, Kargar HMP. New exact traveling wave solution of Fisher Kolmogorov-Petrovskii-Piskunov equation for favorite genes spreading by (1/G)-expansion method. *Journal of Chemical Health Risks*. 2022; 12(3). Available from: https://doi.org/10.22034/jchr.2021.1919624.1243.

[10] Ponraj A, Vaganan BM. A boundary value problem for algebraically accelerated frequency of mutations governed by Fisher-Kolmogorov-Petrovskii-Piskunov equation. *New Mathematics and Natural Computation*. 2025; 1-18. Available from: https://doi.org/10.1142/S1793005726500419.

[11] Ullah I, Shah K, Abdeljawad T. Study of traveling soliton and fronts phenomena in fractional Kolmogorov-Petrovskii-Piskunov equation. *Physica Scripta*. 2024; 99(5): 055259. Available from: https://doi.org/10.1088/1402-4896/ad3c7e.

[12] Khater MM, Attia RA, Abdel-Aty AH, Alharbi W, Lu D. Abundant analytical and numerical solutions of the fractional microbiological densities model in bacteria cell as a result of diffusion mechanisms. *Chaos, Solitons & Fractals*. 2020; 136: 109824. Available from: https://doi.org/10.1016/j.chaos.2020.109824.

[13] Kuo CK. New solitary solutions of the Gardner equation and Whitham-Broer-Kaup equations by the modified simplest equation method. *Optik*. 2017; 147: 128-135. Available from: https://doi.org/10.1016/j.ijleo.2017.08.048.

[14] Akbari M. The modified simplest equation method for finding the exact solutions of nonlinear PDEs in mathematical physics. *Quantum Physics Letters*. 2014; 3(3): 33. Available from: http://dx.doi.org/10.12785/qpl/030302.

[15] Razzaq W, Zafar A, Akbulut A. The modified simplest equation procedure for conformable time-fractional Boussinesq equations. *International Journal of Modern Physics B*. 2022; 36(17): 2250095. Available from: https://doi.org/10.1142/S0217979222500953.

[16] Alfalqi SH, Alzaidi JF, Lu D, Khater M. On exact and approximate solutions of (2 + 1)-dimensional Konopelchenko-Dubrovsky equation via modified simplest equation and cubic B-spline schemes. *Thermal Science*. 2019; 23(Suppl. 6): 1889-1899. Available from: https://doi.org/10.2298/TSCI190131349A.

[17] Raheel M, Zafar A, Cevikel A, Rezazadeh H, Bekir A. Exact wave solutions of truncated M-fractional new hamiltonian amplitude equation through two analytical techniques. *International Journal of Modern Physics B*. 2023; 37(01): 2350003. Available from: https://doi.org/10.1142/S0217979223500030.

[18] Murad MAS, Iqbal M, Arnous AH, Yildirim Y, Jawad AJM, Hussein L, et al. Optical dromions for Radha-Lakshmanan model with fractional temporal evolution by modified simplest equation. *Journal of Optics*. 2024; 1-10. Available from: https://doi.org/10.1007/s12596-024-02201-5.

[19] Achouri T, Ayadi M, Habbal A, Yahyaoui B. Numerical analysis for the two-dimensional Fisher-Kolmogorov-Petrovski-Piskunov equation with mixed boundary condition. *Journal of Applied Mathematics and Computing*. 2022; 68(6): 3589-3614. Available from: https://doi.org/10.1007/s12190-021-01679-7.

[20] Sulaiman TA, Yel G, Bulut H. M-fractional solitons and periodic wave solutions to the Hirota-Maccari system. *Modern Physics Letters B*. 2019; 33(05): 1950052. Available from: https://doi.org/10.1142/S0217984919500520.

[21] Sousa JVC, Capelas de Oliveira E. A new truncated M-fractional derivative type unifying some fractional derivative types with classical properties. *arXiv:170408187*. 2017. Available from: https://doi.org/10.48550/arXiv.1704.08187.

[22] Gu M, Liu F, Li J, Peng C, Li Z. Explicit solutions of the generalized Kudryashov's equation with truncated M-fractional derivative. *Scientific Reports*. 2024; 14(1): 21714. Available from: https://doi.org/10.1038/s41598-024-72610-w.

[23] Farooq A, Ma WX, Khan MI. Exploring exact solitary wave solutions of Kuralay-II equation based on the truncated M-fractional derivative using the Jacobi Elliptic function expansion method. *Optical and Quantum Electronics*. 2024; 56(7): 1105. Available from: https://doi.org/10.1007/s11082-024-06841-6.

[24] Junjua MuD, Mostafa AM, Alqahtani NF, Bekir A. Impact of truncated M-fractional derivative on the new types of exact solitons to the (4 + 1)-dimensional DSKP model. *Modern Physics Letters B*. 2024; 38(32): 2450313. Available from: https://doi.org/10.1142/S0217984924503135.

[25] Veeresha P, Prakasha D, Singh J, Khan I, Kumar D. Analytical approach for fractional extended Fisher-Kolmogorov equation with Mittag-Leffler kernel. *Advances in Difference Equations*. 2020; 2020(1): 174. Available from: https://doi.org/10.1186/s13662-020-02617-w.

[26] Qawaqneh H, Manafian J, Alharthi M, Alrashedi Y. Stability analysis, modulation instability, and beta-time fractional exact soliton solutions to the Van der Waals equation. *Mathematics*. 2024; 12(14): 2227-7390. Available from: https://doi.org/10.3390/math12142257.

[27] Tariq KU, Wazwaz AM, Javed R. Construction of different wave structures, stability analysis and modulation instability of the coupled nonlinear Drinfel'd-Sokolov-Wilson model. *Chaos, Solitons & Fractals*. 2023; 166: 112903. Available from: https://doi.org/10.1016/j.chaos.2022.112903.

[28] Zulfiqar H, Aashiq A, Tariq KU, Ahmad H, Almohsen B, Aslam M, et al. On the solitonic wave structures and stability analysis of the stochastic nonlinear Schrödinger equation with the impact of multiplicative noise. *Optik*. 2023; 289: 171250. Available from: https://doi.org/10.1016/j.ijleo.2023.171250.

[29] Alomair A, Al Naim AS, Bekir A. Exploration of soliton solutions to the special Korteweg-De Vries equation with a stability analysis and modulation instability. *Mathematics*. 2024; 13(1): 54. Available from: https://doi.org/10.3390/math13010054.

[30] Rahaman MS, Islam MN, Ullah MS. Bifurcation, chaos, modulation instability, and soliton analysis of the Schrödinger equation with cubic nonlinearity. *Scientific Reports*. 2025; 15(1): 11689. Available from: https://doi.org/10.1038/s41598-025-96327-6.